Specular and Diffuse Components in Spherical Satellite Photometric Modeling

M.D. Hejduk
a.i. solutions Inc.

ABSTRACT

Simulation efforts to inform investment decisions for future space sensors need a simple method to estimate the photometric behavior of satellites in a postulated future catalogue, generally for the purpose of emulating sensor detectability. Many simulations accomplish this by using the phase function of a diffuse sphere, at least for debris objects and sometimes for all object types. The present study examines other proposed phase functions from debris studies to determine if a competing (but simple) alternative phase function model can render improved fidelity. It also considers the earthshine contribution to satellite brightness and articulates conditions under which this phenomenon needs to be accounted for explicitly. The investigation demonstrated that a considerable improvement in predictive performance can be achieved by using simple models that allow a mixture of diffuse and specular components, although aspects of the results do force the observer to question these models' ultimate adequacy. Guidance on the use of these models in simulations is also provided.

1. INTRODUCTION

Space Situational Awareness (SSA) simulation tools often require estimates of satellite signature information, such as radar cross-section (RCS) and visual magnitude (VM), in order to drive space sensor detectability models. When speculative satellite catalogues are assembled in order to run such simulations against the expected space situation some number of years in the future, they often give for each object only a single average RCS, brightness, or size value; this datum is better than no information at all, but the simulation organization is left with the difficult task of turning this single value into an appropriate input to a detectability model for a given sensor. In the case of photometry, the task is particularly complicated because the satellite photometric response is not simply an intrinsic quality of the satellite (as it essentially is for RCS, even if the quality can be characterized only stochastically) but is dependent on the illumination geometry of the sun-satellite-sensor encounter. Despite this additional difficulty—or perhaps because of it—simulation analysts have chosen a very simple approach: to model all satellites photometrically as diffuse spheres. The advantages of this method from a computational point of view are obvious: there is no variation of photometric return with satellite aspect (as a sphere, the satellite presents the same return in all of its rotational orientations), and its brightness, M_v, is a straightforward deterministic calculation based on the solar phase angle, satellite albedo, and satellite size (here spherical diameter). The governing equation is given for reference below:

$$M_v = -26.74 - 2.5 \log\left(\frac{2}{3\pi^2} A\rho[(\pi - \varphi)\cos\varphi + \sin\varphi]\right) + 5\log(R) \tag{1}$$

in which A is the sphere's cross-sectional area, ρ is the bond albedo, φ is the solar phase (sun-satellite-sensor) angle, and R is the satellite-sensor range-to-target. Even with this level of simplification, one is further waylaid by the need to assign a bond albedo to the satellite, knowing that values for certain satellite construction materials can range from almost zero to as high as 0.5. But if a suitable average albedo value is chosen—a value of 0.17 was advanced by one study as a suitable value for debris objects [1]—then indeed one can move freely between a satellite characteristic dimension (which one takes to be the diameter of the modeled sphere) and a resultant visual magnitude at a given solar phase angle.

Unfortunately, one purchases this ease of transformation only by ignoring the multiple studies that have indicated that a diffuse sphere model is in general a poor choice [2 3 4 5]—it does not reproduce most satellites' phase functions well; and if it cannot even do that, there is little reason to suppose that any additional information it might render, such as estimates of satellite size, would be at all representative. However, while the photometric community has manifested its disapproval of the diffuse sphere solution, it has done rather little to provide an alternative to the simulation community. It is certainly correct to describe the definition of durable satellite

photometric models as a difficult problem; but one cannot deny that the simulation operators need to have some method to assess the trackability of hypothesized catalogues by proposed optical sensor systems, and these simulation operators are looking to the photometric community for algorithmic guidance on this point, even if the results to be offered may be less than fully satisfactory to a specialist. In short, there is a need to provide an improvement to the current *modus operandi*, even if it is far from the definitive solution that the photometric community would find pleasing.

2. PROBLEM STRUCTURE

Satellite photometric response can be divided into three principal components: the albedo, or the amount of reflected light the satellite's materials will return; the satellite aspect, which governs the particular satellite surfaces that the incident light will encounter; and the phase function, which determines the amount of illuminated area that the sensor will observe and can also include the apportionment of specular and diffuse reflection. Of these three components, satellite aspect is probably the most influential but ironically the least important for the present problem, as the satellite-sensor aspect function is in general not known, forcing any brightness solution to be that for an "average" value at a given phase angle. While it may be useful to determine for a given phase angle the amount of brightness variation due to aspect changes, it will almost never be possible to solve for it explicitly. Remaining to be determined are thus the albedo and phase function. Calculating the albedo requires reconstructing the construction materials of a given spacecraft and then determining the scattering properties of those materials in the laboratory, as well as characterizing and correcting for the "space reddening" effect. While the beginnings of both of these efforts have been observed [6 7], a robust campaign will be needed to do this for different classes of satellites. The remaining component is thus the phase brightness function, and for this there is enough prior research and extant photometry data to enable some palpable progress.

A good place to begin such an investigation is through the viewing of empirical brightness versus phase functions for an host of different objects. The Kriging Optimized Interpolation (KOI) satellite brightness prediction model that currently runs at the Joint Space Operations Center (JSpOC) at Vandenberg Air Force Base, CA uses the rather large photometric database from the Ground-Based Electro-Optical Deep-Space Sensing System (GEODSS) system (currently over four million measurements) to produce a graphical brightness-vs-phase plot for each object; the viewing of a large number of these plots, spanning all the different satellite classes, can give a sense of the different phase-dependent brightness behaviors actually observed [8 9]. A previous study effort examined these empirical data and attempted to classify the different strains of behavior, often by fitting a straight line to the data and using the slope and fit residuals as characterization parameters [10]. One important result from this study is that phase functions do not conform to a narrow range of behaviors but present both intuitive and counter-intuitive results, in both a well-behaved and noisy manner. Any sort of deterministic function used to represent brightness-vs-phase behavior will be a compromise, and situations—even well-sampled ones—will be encountered that simply cannot be represented by intuitive functions. At the same time, curve-fitting to any convenient function, while a useful descriptive exercise, is not ultimately helpful because no link is preserved to a paradigmatic object whose characteristic dimension might be extracted from the functional results, nor would the result have any real basis in physics. Phase functions must be chosen that maintain a link to real satellite structures and thus articulate a relationship among size, albedo, and brightness.

3. PHASE FUNCTIONS

An initial assembly of candidate phase functions is proposed in Mulrooney's study of the phase functions of fragmentation debris [11]. Although the datasets were small and somewhat constrained in the breadth of phase angles available, the study nonetheless was able to demonstrate that this object class could be reasonably represented by two different spherical phase function mixtures. The first of these was the combination of the classical diffuse and specular spheres through a mixing coefficient β; this model will be called the "diffuse-specular" model:

$$F_1(\varphi) = \frac{2}{3\pi^2}\left[(\pi - \varphi)\cos\varphi + \sin\varphi\right] \tag{2}$$

$$F_2(\varphi) = \frac{1}{4\pi} \tag{3}$$

$$M_v = -26.74 - 2.5\log(A\rho[\beta F_1(\varphi) + (1-\beta)F_2(\varphi)]) + 5\log(R) \qquad (4)$$

in which F_1 is the diffuse sphere phase function, F_2 is the specular sphere phase function, and M_v is the resultant brightness. Other variables include φ as the satellite-sun-sensor solar phase angle (in radians), A as the cross-sectional area, ρ as the bond albedo, and R as the range to target. In this formulation, a value of $\beta = 1$ would represent a purely diffuse sphere and a value of $\beta = 0$ a completely specular sphere. As few objects are purely diffuse or purely specular reflectors, the idea of a combined response described by a proportional mixing coefficient is quite reasonable. The second class involves the introduction of the lunar brightness model given in Allen [12]. It has long been remarked that the full moon is substantially brighter than a diffuse sphere under similar conditions, especially around the edges of the sphere, which should fall off in brightness much more strongly if the moon were purely a diffuse reflector. It has been surmised that the lunar surface, which is both dusty and pitted, has very small faceted components that increase the specular response but in a way different from what would be predicted strictly from the geometry. A quadratic fit to the empirical lunar phase function presented in Allen [12], taken from Mulrooney [11], is given below (φ in degrees); this model will be called the "diffuse-lunar" model.

$$F_3(\varphi) = \frac{5}{\pi^2}\left[(5.3095E{-}05)\varphi^2 - (1.2591E{-}02)\varphi + 0.79121\right] \qquad (5)$$

To calculate actual brightnesses using this phase function, F_3 above is substituted for F_2 in equation (4), after
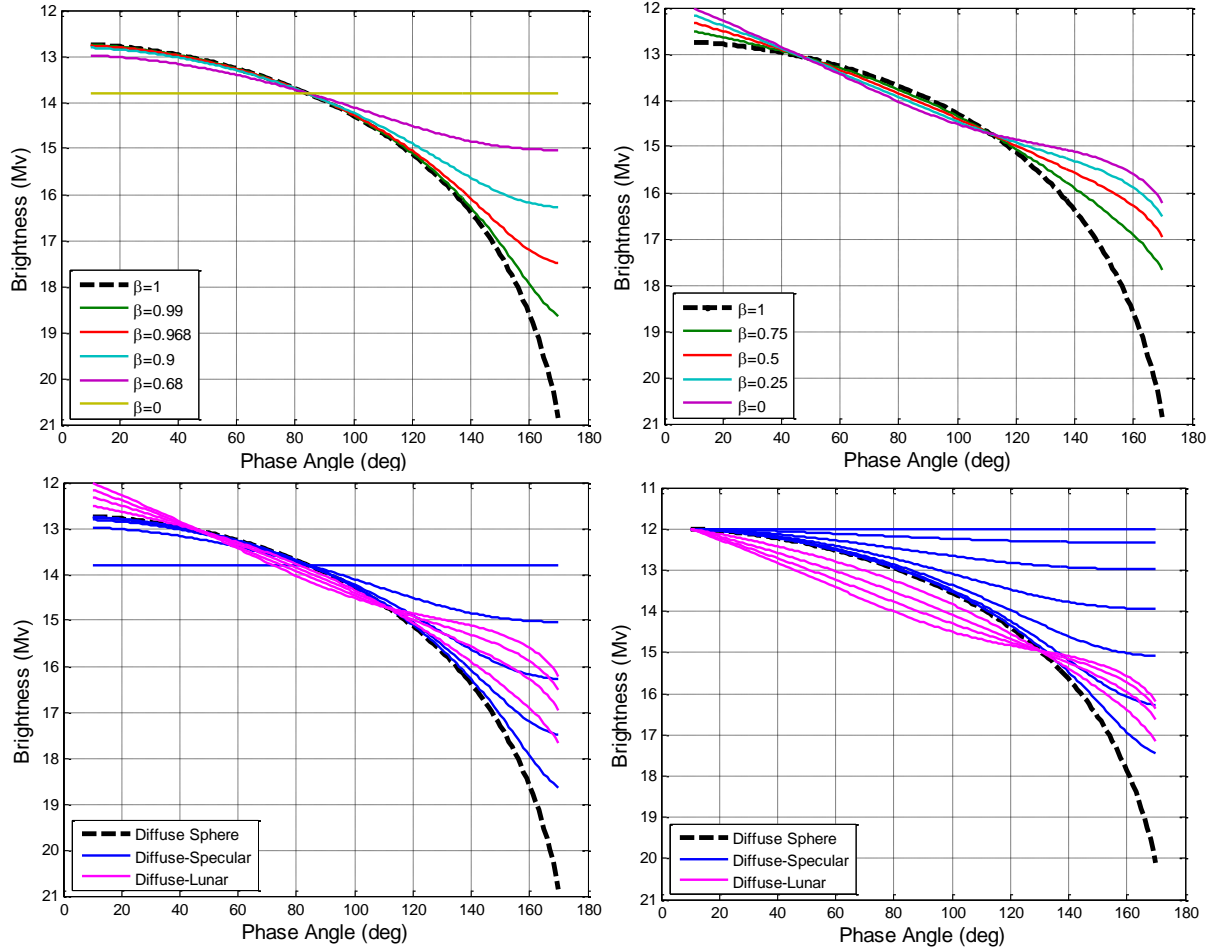

Fig 1: **Behavior of the two different mixture phase functions. Numeration begins at upper left (pane A) and proceeds clockwise. Panes A, B, and D are generated with a albedo-area product of unity; pane C normalizes all of the curves to have a zero-phase brightness of 12 Mv**

normalizing it to unity so that it renders flux per unit solid angle.

The comparative behavior of these different phase functions can be seen in Fig. 1, which show performance of all models at a nominal observing range of 36,000 km. Pane A gives results for the diffuse-specular sphere combination at different values of β. The contrast between the constant response of the specular sphere (β=0) and the almost 8-M_v trail-off of the diffuse sphere (β=1) as the phase angle moves from 10 to 170 degrees is striking, but it is also interesting how small of a specular component (10%; β=0.90) will constrain the trail-off to a mere 3 M_v. Pane B shows a similar range in β for the lunar phase function. This function maintains a more consistent slope over the full range of β, at least until one approaches the fully diffuse case (β=1); both families (diffuse-specular and diffuse-lunar) of course give the fully diffuse sphere response at β=1 (black hashed lines). Panes C and D plot both curve families on the same axes, with the full range of β mixing coefficients for each. From looking merely at these canonical plots, it is not obvious whether both families will truly be necessary to describe the phase functions of actual objects, as there are areas of the superimposed plotting where both curve-sets are very similar.

4. EARTHSHINE

Nearly all of the study of satellite photometry to date has drawn upon datasets taken from ground-based sensors. Because these sensors must be in darkness in order to observe any significant dynamic range of satellite brightnesses, solar phase angles are generally limited to less than about 120 degrees. This is simply a consequence of the geometries that arise if the sensor is to remain in darkness and the satellite is to be observable at a height greater than the minimum elevation possible for most telescopes. In such a case, the contribution of earthshine to a satellite's brightness is essentially negligible because the satellite is not in a position to reflect any appreciable illumination from the illuminated earth back towards the sensor. As the phase angle becomes larger, however, the situation changes, with the earthshine component becoming more and more significant until the phase angle value of 180 degrees is reached: at this point the sun does not contribute anything to the illumination of the satellite as seen from the earth, but the reflected earthshine could contribute quite a bit. Of course, a ground-based telescope could not benefit from such a situation because it would arise at the telescope's local noon; but a space-based sensor would have no such inherent restriction—its limitation would be governed only by how close to the sun it could observe. Because space-based concepts have been proposed that can observe as close as eight degrees to the sun, the contribution of earthshine to satellite photometry now needs to be considered explicitly.
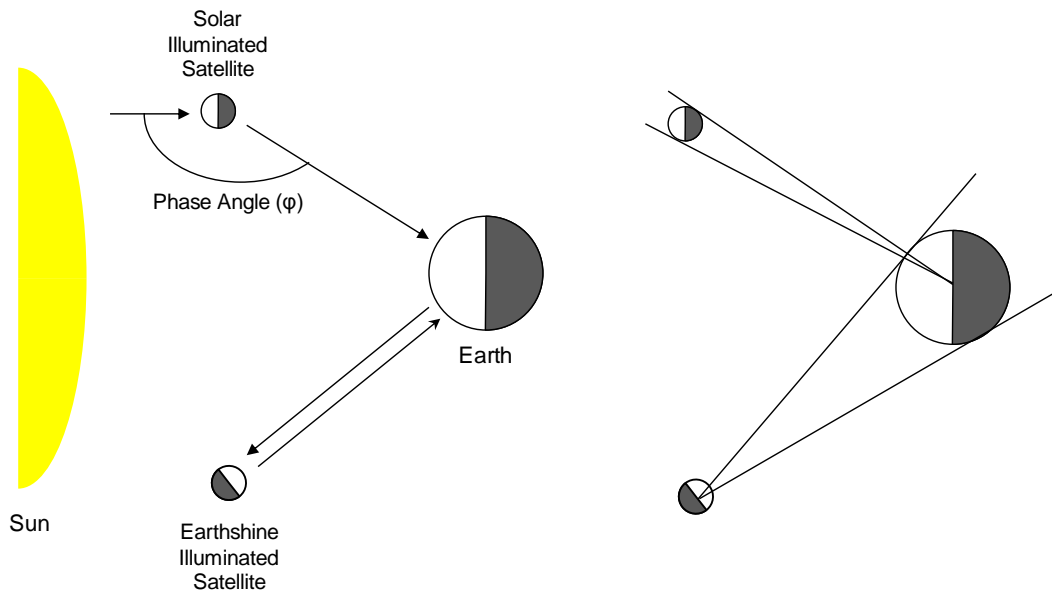

Fig. 2: Comparison of solar- and earthshine-illuminated geometries

The geometry of the situation is shown in Fig. 2. The upper part of the left side shows the usual arrangement for a solar-illuminated satellite, except here the solar phase angle (φ) is very large—about 150 degrees. Very little of the satellite's solar-illuminated surface can be seen from the earth, as the cone drawing in the upper part of the right

side reveals. Such an observing situation is probably not actually possible from the earth for a telescope that itself is in darkness. The bottom part of the diagram describes the situation for which the satellite is illuminated by earthshine. For an observing platform on the earth or close to the earth (such as a satellite in low-earth orbit observing satellites at a geosynchronous orbit), the illuminated side of the satellite faces the earth directly; but the portion of the illuminated earth that actually can illuminate the satellite changes; in fact, it is dictated by the inverse of the solar phase angle $(180 - \varphi)$. The right side of the bottom part of the figure shows the cone diagram for this case, in which most of the surface of the earth visible to the satellite is in illumination. Of course, this phase angle inversion identity is only approximate because the earth as a source of illumination is much closer to the satellite than is the sun and cannot truly be represented as a point source located at its center of mass, but this identity—that the complement of the solar phase angle $(180 - \varphi)$ serves as the governing illumination angle for the earthshine case—is certainly adequate for a first-order model.

Allen [12] provides basic photometric data for planets and satellites, and his table gives parameters to represent the earth as a diffuse uniform reflector with an illumination brightness of -21.6. Combining this with the phase-angle identity described above modifies equation (4) to give the expected observed brightness due to earthshine:

$$M_v = -21.6 - 2.5\log(A\rho[\beta F_1(\pi - \varphi) + (1 - \beta)F_2(\pi - \varphi)]) + 5\log(R) \qquad (6)$$

with φ as the solar phase angle in radians from equations (2) - (4). A more elaborate "planet-shine" model was developed in [13] in order to assist the discovery of earth-like planets as part of the NASA Terrestrial Planet Finder mission. The authors do not provide the model in its fullness so that one can run it personally, but they do give a diagram that compares its output (green curve) to a set of earthshine observations [14] (blue x's) and the modeling of the earthshine as a diffuse sphere (red curve), reproduced here (with less than desirable reproduction quality, unfortunately) in Fig. 3:
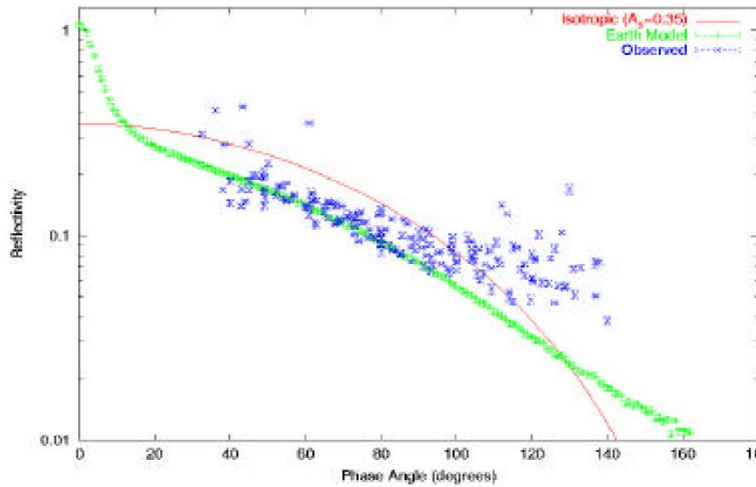

Fig. 3: Higher-fidelity earthshine model compared to observations and diffuse sphere (from [13]). The y-axis represents reflectivity (log scale), and the x-axis represents the solar phase angle in degrees

In truth, neither of the two models seems to fit the observed data all that well, but somewhat better performance can be claimed for the higher-fidelity model. It is not known whether the extremes of the higher-fidelity model represent reality, as there are no observations in those regions for comparison; but in the main part of the data area the reflectivity difference between the red and green curves does not exceed a factor of two, which is equivalent to 0.75 of a visual magnitude of brightness; and over much of the phase-angle span the difference is less than this. Given this bounded and not excessively large difference, the representation of the earth as a diffuse reflector can be claimed to be acceptable as a first-order model.
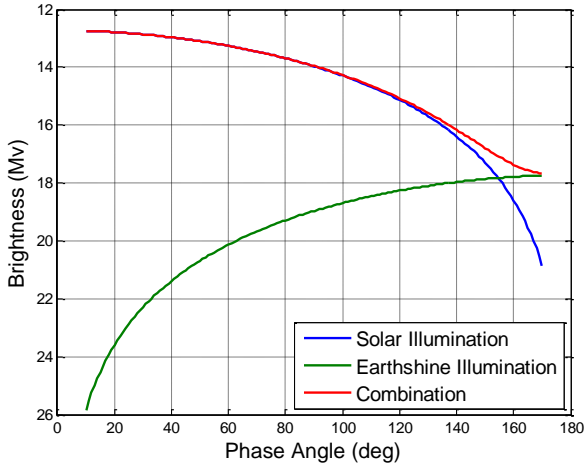
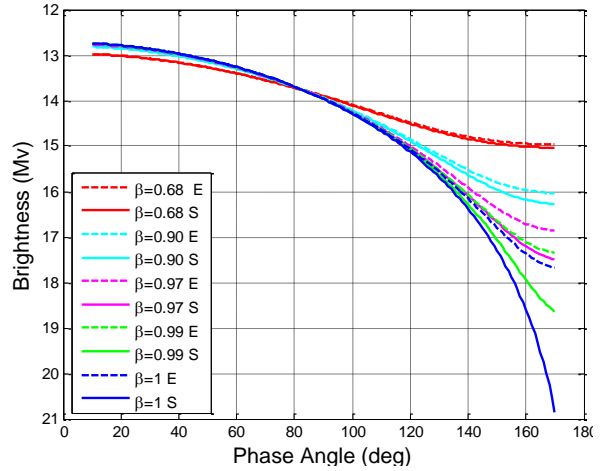**Fig. 4: Contribution of earthshine to diffuse sphere brightness**

Fig. 5: Photometric response with and without earthshine for different values of β

How much of an effect does the consideration of earthshine have on the overall brightness? Fig. 4 shows, for a diffuse sphere with an albedo-area product of unity, the brightness contributions of the solar illumination (blue line), the earthshine illumination (green line), and the combined brightness (red line). For phase angles less than 130 degrees, the earthshine contribution is so dim that is it entirely negligible; and its contribution does not add a full visual magnitude until a phase angle of about 150 degrees. So for phase angles less than 140 degrees or so, one can safely ignore the earthshine effect. Given that the largest phase angles in the dataset used in the present analysis (described in Section 5 below) are 125 degrees, it is quite acceptable to ignore the earthshine contribution in fitting empirical phase functions to the models proposed in Section 3. If, however, one does wish to consider the earthshine contribution in the diffuse-specular mixed case, as set out in equation (4), the differences between the models that include earthshine (marked with an "E" in the legend) and those that do not ("marked with a "S"), are given in Fig. 5. Here, one can see that as the specular component becomes larger, the brightness contribution from the earthshine becomes less significant; for example, with a specular component as small as 10% (β=0.90, aqua line in Fig. 5), the brightening due to earthshine at a 160-degree phase angle is only about 0.2 M_v—a relatively small amount. It is thus only when the diffuse component is very large—perhaps in the 95% to 97% range (β=0.95 to 0.97)—that the brightness decrement becomes large enough to mandate the application of an offset, and then of course only at the highest of phase angles.

5. DATASET AND PHASE FUNCTION FITTING PROCEDURES

The GEODSS optical tracking system records a photometric brightness measurement with each metric track taken; it is this photometric database, begun in 2006 and, as previously mentioned, consisting of approximately four million measurements, that was made available for the present study. Each GEODSS tracking frame is photometrically calibrated against solar-equivalent registration stars, a procedure that is believed to yield a photometric accuracy better than 0.3 Mv.

Objects were considered for curve-fitting only if they possessed over 300 individual photometric measurements and thus could be considered well tracked; 2200 such deep-space objects existed in the GEODSS photometric database and were thus available for examination. Because the different phase functions differ most strongly at their extremes (low and high phase angles), a binning procedure in which the brightness data for each satellite are divided up into phase-angle bins, and the median value for each bin is used to drive the curve-fitting, is appropriate. This method prevents the areas of high data density, which are usually away from the extremes of the phase angle range, from dominating the curve-fitting results. Five-degree phase bins were used, centered from 2.5 degrees to 122.5 degrees; it was required that a bin possess at least five measurements in order to be considered in the fitting routine. Ninety percent of the 2200 objects produced 19 or more defined bins, and 99% produced at least 16 defined bins.

The two curve families to be applied to each candidate satellite each have two free variables: the albedo-area product ($A\rho$ in equation 4) and the mixing coefficient β; and these equations are non-linear in these variables. An

expeditious solution procedure is to divide the reasonable values of these two variables to a suitable granularity, try all of the combinations of these variables in the proposed models, calculate residuals for each of these combinations against the datasets for each satellite, and identify the model and parameters that produces the best modeled result for each satellite. One-percent increments were used in varying the mixing parameter (in MATLAB notation, β=0:01:1), and a logarithmic scaling was used for the albedo-area product (in MATLAB notation, 10.^(-4:0.01:1.5)). For each combination, the residual root-mean square (RMS) was computed and retained. Because fit performance at the tail-ends of the phase function curves is the more discerning indicator of the appropriate phase function, the RMS (which would impose a heavier penalty for larger divergences, which are likely to be in these tails) is a more attractive choice of fit cost function over a more ecumenical alternative, such as median-square error. For each satellite examined, the results for both mixed model and both extremes of the diffuse-specular model (β=1 for purely diffuse sphere and β=0 for purely specular sphere), including the mixing coefficients, fit RMS, and albedo-area product, are preserved.

Fit results are separated by satellite object type, as it is of interest which phase functions are more appropriate to debris or intact spacecraft. The following object type definitions were used in this analysis:

Table 1: Object Type Category Definitions

Object Type	Definition
Stabilized Payload	A geosynchronous intact spacecraft that is able to maintain a fixed orbital longitude position and thus maintains an invariant aspect with respect to a ground sensor. A stabilized payload is defined as one that maintains a longitude drift rate of less than 0.03 degrees/day
Other Payload	A non-stabilized GEO intact spacecraft, or any intact spacecraft outside of the geosynchronous region; all such objects will present a varied aspect to a ground sensor
Rocket Body	Self-explanatory
Fragmentation Debris	Debris that was generated by an actual fragmentation event, as opposed to spacecraft offscourings or launch- or deployment-related detritus
Other Debris	Debris objects not generated by a fragmentation event

5. FIT RESULTS

One obvious feature of the canonical phase function curves presented in Fig. 1 is, except for the unusual case of the purely specular sphere, the decreasing brightness with increasing phase angle. While this general relationship is observed in most cases, it is not present in all. Fig. 6 shows a cumulative distribution function (CDF) plot of the slopes of a least-squares linear fit through the binned brightness data for each object—this type of CDF plot is essentially a numerical integration of a histogram and gives cumulative probability (percentage) as a function of a parameter's increasing value. For payloads and rocket bodies, nearly all of the fits have a positive slope (decreasing brightness with increasing phase). For debris objects, however, there is a non-negligible number of cases that manifest the reverse phenomenon, and some of these slopes cannot be said to be near zero. There is no simple and
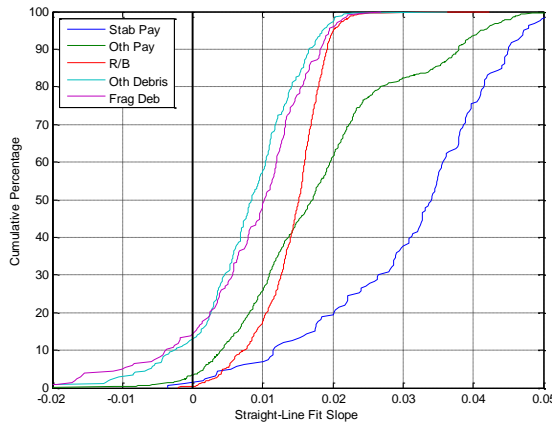

Fig. 6: Slopes of straight-line fits to binned brightness data, by object type

satisfying explanation for this behavior among debris objects, for which systematic brightness variations due to a fixed satellite aspect function are not really possible. Not only will these cases not perform well against the candidate models under examination here, they will actually distort the results; for these cases will, for lack of a better candidate, always advance the specular sphere (β=0, constant brightness with phase angle) as the winning model type, when these objects are certainly not highly polished spheres and manifest a brightness that is not constant but that actually increases with increasing phase angle. It thus makes sense for the present analysis to remove these curious objects from consideration and address them in a future investigation. Table 2 presents statistics on the "winning" phase function models, delineating results by object type. The table provides both

unfiltered results (the "before" case) and results with the negative-slope cases removed (slope less than -0.002, with a small amount of negative slope allowed in order to preserve the "straight-line" cases that might fit the specular sphere). A good number of specular sphere fits disappear once the pathologies are removed. One observes that, overall, debris is well modeled by the diffuse-specular mix (80%-85% of the debris objects), about two out of three rocket bodies are better modeled by the diffuse-specular mix (a somewhat surprising result), non-stabilized payloads split evenly between the two mixture models, and stabilized payloads perform substantially better with the diffuse-lunar model (85%). Each model type seems to have particular object types for which it performs more strongly.

Of course, one wonders just how "specular" or "lunar" these winning composite functions are—what is the distribution of mixing coefficients that is actually produced. Fig. 7 provides CDF plots of this parameter by object

Table 2: "Winning" phase function models, by object type. Each column sums to 100%. "Before" and "After" indicate before and after pathological cases were removed

	Satbilized Payloads		Other Payloads		Rocket Bodies		Other Debris		Fragmentation Deb	
	Before	After	Before	After	Before	After	Before	After	Before	After
Diffuse Sphere	1.21	1.22	0.13	0.14	0.83	0.83	0.38	0.42	0.99	1.12
Specular Sphere	1.21	0.61	3.64	1.92	0.28	0.14	12.83	2.53	14.78	3.35
Diffuse-Specular	12.73	12.80	46.29	47.12	68.83	68.92	75.85	84.81	69.46	78.77
Diffuse-Lunar	84.85	85.37	49.93	50.82	30.07	30.11	10.94	12.24	14.78	16.76

type. With the exception of rocket bodies, objects that are best represented by the diffuse-specular model (left graph) produce an almost uniform distribution of the mixing coefficient—the curves track very close to the "y=x" line on the CDF plot. All of the different levels of specular versus diffuse response are observed with more or less equal frequency for the objects that embrace this model, again with the exception of rocket bodies, which show notably more diffuse reflection behavior than even debris. This overall result is surprising, as it was expected that a greater proportion of the objects would show more diffuse behavior. The situation for the diffuse-lunar mixing case (right graph) is less homogeneous. The non-payload object types are clustered and more diffuse than was observed with the diffuse-specular model, with over half of the debris and rocket bodies rendering greater than 80% diffuse response. On the other hand, the payloads, especially stabilized payloads, are remarkably "lunar," with 40% of the dead payloads and a remarkable 70% of the stabilized payloads rendering full lunar-type specular response.
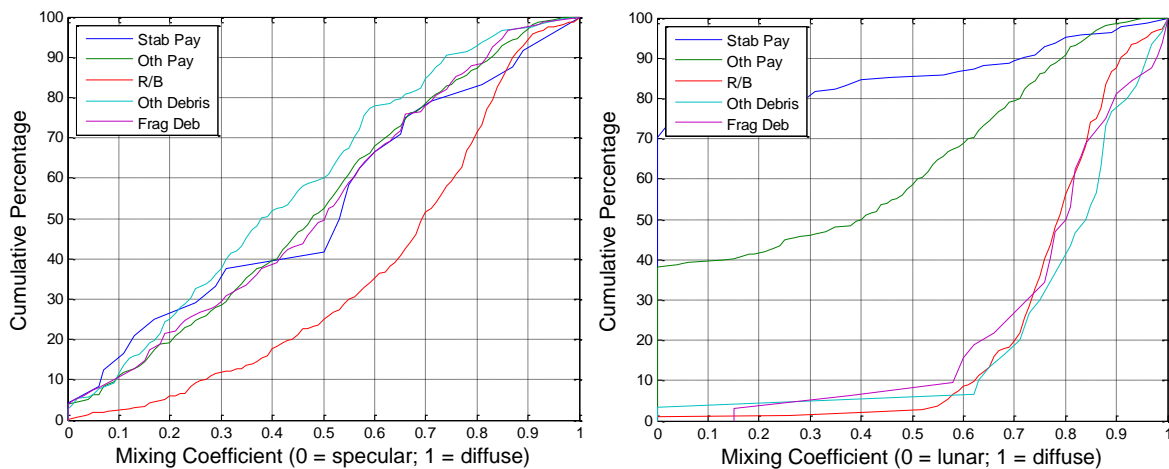

Fig. 7: Mixing coefficient distributions for winning phase functions. Left graph is for the diffuse-specular sphere; right graph represents the diffuse-lunar sphere

These results cannot be seen as particularly sanguine for either model. For the diffuse-specular case, the uniform distribution of mixing coefficients across all object types leads the analyst to wonder whether the combination of a diffuse and specular spherical model represents the objects' photometric response in any physically meaningful way. One can certainly create models and fit data to them, just as one can pursue curve-fitting not deriving from any consideration of the physics of the situation; but the fact that very different object types, from

fragmentation debris to stabilized payloads, all run the entire length of possibilities for the mixing coefficient with about equal probability suggests that the model inherently is not capturing the features distinctive to the different object types, and therefore probably not for the objects in general. For the diffuse-lunar case, the relatively small number of non-payloads that become assigned to this model are more constrained in their behavior (most have a diffuse component exceeding 70%), but large portions of both the stabilized and unstabilized payload population are assigned a mixing coefficient of zero. While it is possible that full lunar response (which is what a mixing coefficient of zero would indicate) is a very good fit for those particular satellites, it is far more likely that these satellites have a peaked specular response at low phase angles—the assignment of full lunar response is simply the closest the model can come to the satellites' actual photometric presentation and in and of itself may not be all that representative. When no "ground truth" exists for a modeling effort such as this, one must look to model coherence to give clues about model adequacy. Here, the clues are not encouraging: a uniform distribution of mixing coefficients in one case and a large number of extreme values of the mixing coefficient in the other.
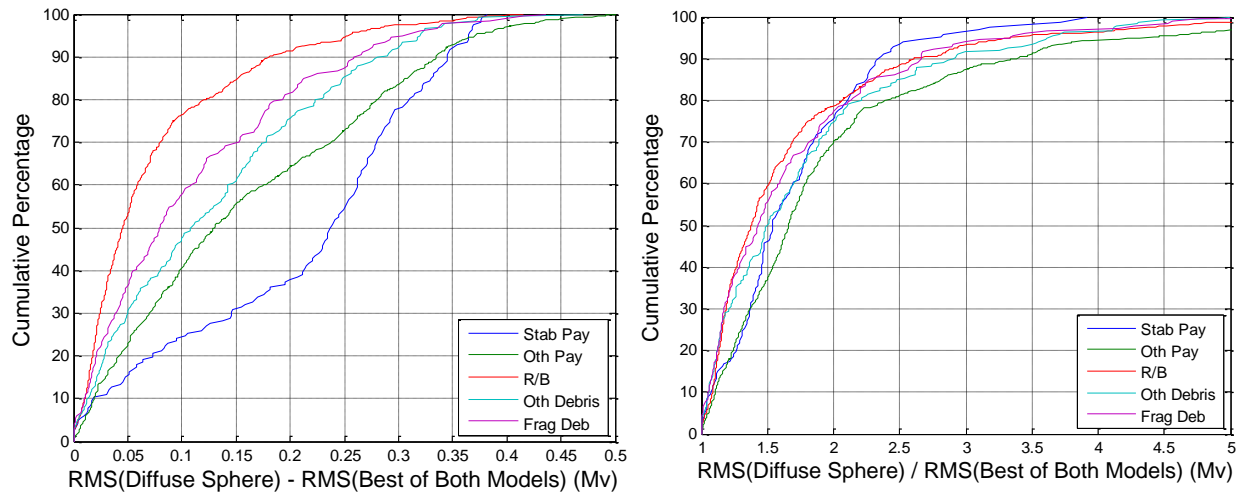

Fig 8: Comparative performance of both models to the diffuse sphere. Left graph shows the linear RMS difference; right graph the RMS ratio

But while the absolute rectitude of the models cannot be decisively evaluated, what can be established is the degree of their superiority over using only a diffuse sphere model (effectively setting the mixing coefficient of either model to unity). Fig. 8 gives CDF plots of the RMS differences between the winning model assignment and a simple diffuse sphere model; these data are plotted both as absolute differences and as ratios. Between 20% to 30% of all object types show a factor of two or better improvement in RMS, and the absolute values of these improvements are not negligible (*ca.* 0.2 M_v or greater)—both of these factors indicate consistent superior fitting with the mixed models. It is not surprising that those object types found to be most specular (payloads) benefit the most from moving beyond the diffuse sphere model. Fig. 9 places these data in the context of a brightness difference at a large phase angle; the angle chosen here was 140 degrees, a large angle but not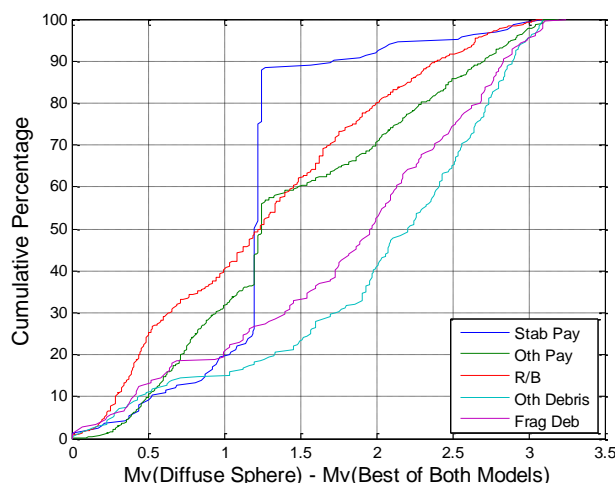 large enough to require compensation for earthshine. Because it is in the region of high phase angles that the different models differ the most, the full effect of a model mis-selection is most strongly in evidence here. At the 50th percentile, one observes brightness differences ranging from 1.5 to over 2 M_v—a considerable difference. A brightening by this amount can significantly reduce the needed

Fig 9: Brightness differences between best model and diffuse sphere at 140 deg phase angle

telescope size and/or performance necessary to track successfully in these situations and thus decrease system cost. The strong spike in the stabilized payload CDF curve is simply the difference between a diffuse sphere and a fully lunar modeling at a phase angle of 140 degrees; this same phenomenon appears in the right graph of Fig. 7 as the large number of objects with an assigned mixing coefficient of zero. It is interesting that debris objects, which have generally been thought to be more diffuse than specular reflectors, show such large differences in performance between the mixed models and the diffuse sphere model; clearly the specular component is an important part of their photometric modeling.

6. CONCLUSIONS AND FUTURE WORK

Four main conclusions can be drawn from the present analysis:

1) The earthshine contribution to satellite photometric response can be significant at large phase angles for diffuse reflectors but probably can be safely neglected for objects that have a specular component of 10% or larger. For objects that are more than 90% diffuse, one should consider compensation for earthshine at phase angles greater than perhaps 150 degrees.
2) The diffuse-specular and diffuse-lunar mixing functions are easy enough to apply and give good results. However, certain aspects of the behavior raise doubts about the models' adequacy. The fact that the mixing coefficients for the diffuse-specular model essentially follow a uniform distribution over their full range values (zero to unity) for all object types suggests that this model is not capturing the distinctive features of different strains of satellites. Similarly, the assignment of the great majority of stabilized payloads and a substantial number of all other payloads to the lunar model with a mixing coefficient of zero indicates that the parameter span for this model is not adequate to represent these object types. It would in fact be surprising if a spherical model were able to represent all the different satellite object types well, but problems are observed here even for debris, the presumed most hospitable case for the this model type.
3) Nonetheless, both mixed phase function models significantly outperform a simple diffuse sphere model in terms of improved fit RMS, and these differences translate at a phase angle of 150 degrees to a decrement of 1.5 visual magnitudes (at the 50th percentile) for payloads and rocket bodies and 2 visual magnitudes for debris. There is thus a compelling case to switch from a diffuse sphere model (presently in use in the industry) to the mixed-sphere model set proposed here.
4) For most investment decision simulations, future increases in catalogue size are due either to fragmentation events or the ability to see more pre-existing fragmentation debris (and, to a degree, other debris) due to more capable sensors. Other object types, such as payloads and rocket bodies, are generally large enough that they will be optically bright and thus detectable by most proposed sensors; so the fidelity with which their photometric response is modeled need not be high. Therefore, it would be adequate for the photometric modeling for these simulations to use simply the diffuse-specular mixing model, as it is the model of choice for about 80% of the debris objects. The mixing coefficients can be assigned from a random draw from a uniform distribution. Of course, it remains to be established that debris below the current thresholds of detection follow the same reflectivity properties as those presently under track; but in the absence of a study of these faint objects, the presumption of analogous behavior is reasonable. It is certainly superior to the uncritical use of the diffuse sphere model.

While the approach outlined in 4) above may be an improvement over current industry practice, it is suggestive from the discussion in 2), at least to this author, that the spherical modeling approach, both with a mixed diffuse and specular response and with the lunar variant, is not a satisfactory methodology, even for quasi-stochastic applications that attempt to create entire catalogues of hypothetical satellites rather than model individual objects with fidelity. It is not clear whether adding other Pythagorean solids, introducing "ball-and-stick" satellite models, or having to resort to even more elaborate constructs will be necessary to address this problem in a way that is at all satisfactory. It would seem that the logical way forward would be to re-execute the present analysis with a series of additional models of simple shapes, each with specular and diffuse reflective properties that can be varied, to see if a significant improvement in model predictive force can be achieved, especially for debris. Undoubtedly adding additional models will improve the situation at least slightly, but what is desired here is a degree of improvement that would justify the additional complexity and produce model results that suggest that the basic photometric physics of each of the different object types have been captured.

7. ACKNOWLEDGEMENTS

8. REFERENCES

1. Mulrooney, M.K., Matney, M.J., Hejduk, M.D., and Barker, E.S., "An Investigation of Global Albedo Values," 2008 AMOS Technical Conference, Kihei, HI. September 2008.
2. Lambert, J.V., "Interpretation of Geosynchronous Satellite Phase Angle versus Magnitude Relationships", Contract F05603-90-C-0010 Specialized Data Report: MOTIF FY95-01, 30 NOV 1994.
3. Lambour, R.L., "Phase Angle Dependence of Satellite Brightness Derived from Space-Based Visible Data", MIT/LL Project Report SPC-8, 20 FEB 2001.
4. Lambour, R.L. and Sayer, R.W., "ETS Measurements of Satellite Phase Curves at High Phase Angles", MIT/LL Project Report ETS-138, 12 SEP 02.
5. Hejduk, M.D. "Phase Functions of Deep-Space Orbital Debris." 2007 AMOS Technical Conference, Kihei, HI. September 2007.
6. Cowardin, H.M. "Characterization of Orbital Debris Objects over Optical Wavelengths via Laboratory Measurements." Ph.D. diss., University of Houston, 2010.
7. Abercromby, K. *et al.* "Components and Ground Truth Spectral Measurement Comparisons of FORMOSAT III." 2006 AMOS Technical Conference, Kihei, HI. September 2006.
8. Okada, J.M. and Hejduk, M.D. "Satellite Brightness Estimation using Kriging Optimized Interpolation." 2005 AMOS Technical Conference, Kihei, HI. September 2005.
9. Hejduk, M.D., "Satellite Photometric Modeling using Kriging Optimized Interpolation (KOI)." AFSPC/A9A Technical Report, 1 SEP 09.
10. Hejduk, M.D. "Phase Functions of Deep-Space Orbital Debris." 2007 AMOS Technical Conference, Kihei, HI. September 2007.
11. Mulrooney, M.K. "Optical Phase Functions and Albedos of Orbiting Debris Objects." Master's thesis, Rice University, 1993.
12. Allen, C.W. *Astrophysical Quantities*. Third Edition. London: The Athlone Press, 1973.
13. Seager, S., Ford, E.B., and Turner, E.L. "Characterizing Earth-Like Planets with Terrestrial Planet Finder." Future Research Direction and Visions for Astronomy. Edited by Dressler, A.M. *Proceedings of the SPIE*, Vol. 4835, pp. 79-86 (2002).
14. Goode, P.R., Qui, H., Yurchyshyn, V., Hickey, J., Chu, M.C., Kolbe, E., Brown, C.T., and Koonin, S.E. "Earthshine Observations of the Earth's Reflectance." *Journal Of Geophysical Research and Letters* 28 (2001), pp. 1671-1674.